NUMERICAL INVESTIGATION ON COOLING PERFORMANCE OF RANQUE-HILSCH VORTEX TUBE

by

Hassan POURARIA * ***and Warn-Gyu PARK***
School of Mechanical Engineering, Pusan National University, Busan, Korea

Original scientific paper
DOI: 10.2298/TSCI120610052P

A Ranque-Hilsch vortex tube is a mechanical device that separates a high pressure gas stream into low pressure hot and cold streams. In this study, four different two equation turbulence models namely the standard k-ε, RNG k-ε, Realizable k-ε, and Standard k-ω models were compared to identify the appropriate turbulence model for studying the energy separation effect in a Ranque-Hilsch vortex tube. Comparison between the numerical and experimental results indicates that the Standard k-ε model is better than other models in predicting the energy separation phenomenon. The distributions of temperature, pressure, and components of velocity have been obtained in order to understand the flow behavior inside the tube. The effect of cold outlet diameter on temperature drop and refrigeration capacity was studied. The effect of cold mass fraction on the movement of stagnation point and refrigeration capacity has been investigated. Moreover, the feasibility of improving the cooling performance of vortex tube using the cooling system was investigated. The present numerical results revealed that using the cooling system, the net energy transfer rate from cold inner region to the hot peripheral region increases, thereby improving the cooling performance of the device.

Key words: *vortex tube, CFD simulation, energy separation, turbulence model, cooling performance, refrigeration capacity, cold outlet, stagnation point, cooling system*

Introduction

A Ranque-Hilsch vortex tube (RHVT) is a simple device that produces hot and cold flow from a high pressure gas. Figure 1 shows a schematic diagram of a RHVT [1]. Compressed gas enters the RHVT via one or more tangential nozzles that are placed on one side of the tube and attains a high swirl velocity. The high swirl velocity produces rotational flow inside the tube. This rotational flow moves to the other side of the tube. A part of the gas exits from the hot outlet at the end of the tube; however, adjusting the con-

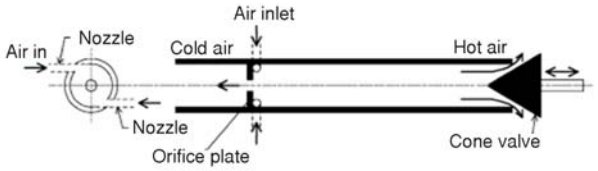

Figure 1. Schematic diagram of a Ranque-Hilsch vortex tube [1]

* Corresponging author; e-mail: pouraria@pusan.ac.kr

trol valve downstream of the hot outlet, causes the other part of the gas to reverse its flow and exit from the cold outlet, which is placed on the same side as the inlet nozzles. The total temperatures of the streams of gas leaving through the hot and cold outlets are higher and lower, respectively, than the inlet temperature. This effect is referred to as the energy (temperature) separation effect. This device was first discovered by Ranque in 1933 [2]. Later, a comprehensive study on the geometrical and performance parameters of this device was carried out by Hilsch [3].

Owing to the numerous advantages of a RHVT over normal commercial refrigeration devices, it has found applications as an appropriate device for heating and cooling gases [1], liquefying natural gases [4], cooling equipments in laboratories [5], cooling for low temperature magic angle spinning [6], and other purposes. Although RHVT has a simple geometry, the energy separation phenomenon that occurs in this device is quiet complex. Many researchers have studied the energy separation effect in a RHVT and have considered different factors in order to explain it. Among the proposed reasons, the pressure gradient and energy transfer due to shear work and heat transfer are more popular than the others. The flow field in a RHVT involves a strong recirculating flow, and the presence of experimental instruments affects the flow field, thereby occasionally leading to opposite conclusions. Recently, by using computational fluid dynamics (CFD), some researchers have studied the energy separation effect in a RHVT.

Frohlingsdorf and Unger [7] used CFX code with k-ε model. Aljuwayhel *et al*. [8] investigated the energy separation effect by using the Standard k-ε and RNG k-ε models. They found that the work transfer between cold and hot regions plays an important role in the energy separation effect and observed that the results from the Standard k-e model were closer to the experimental results when compared to the results from the RNG k-ε model. Skye *et al*. [9] used the Standard k-ε and RNG k-ε models, their results also suggested that the Standard k-ε model is more effective in predicting the energy separation phenomenon than the RNG k-ε model. Behera *et al*. [10] used the RNG k-ε model and investigated the effect of size, shape, and number of nozzles on the performance of a RHVT. Eiamsa-ard and Promvonge [11] used the algebraic stress model (ASM) and the Standard k-ε model and observed that the results obtained from the ASM model were closer to the experimental results. Farouk and Farouk [12] used large eddy simulation (LES) technique for modeling the RHVT used by Skye *et al*. [9], and their predictions indicated that the LES model is more accurate when compared to the Standard k-e model. However, the geometry and boundary conditions used in their model were different from those used in experiment. Hossein Nezhad and Shamsoddini studied the energy separation effect in RHVT by using RNG k-ε model [13, 14]. Their studies about the effect of the number of nozzles indicated that as we increase the number of nozzles the results of 2-D axisymetric model agree very well with the corresponding 3-D modeling. Bramo and Pourmahmoud [15-17] used the Standard k-ε model to study the effect of length to diameter ratio on the performance of a RHVT. Secchiaroli *et al*. [18] used the RNG k-ε model, Reynolds stress model (RSM) and large eddy simulation for studying the flow-field inside a vortex tube. According to their study, the numerical results obtained by RNG k-ε model were different from those obtained by LES and RSM models. Pourmahmoud *et al*. also investigated the effect of helical nozzles on cooling performance of vortex tube [19, 20]. Dutta *et al*. [21] used a 2-D axisymetric domain along with different turbulence models to study the energy separation effect in the vortex tube used by Behera *et al*. [10]. They observed that the numerical results obtained by the Standard k-ε model were closer to the experimental data compared to the other two-equation turbulence models. Furthermore, the 2-D axisymetric results obtained by the Standard k-ε model were more accurate than the published 3-D results obtained by RNG k-ε model [10]. Pouraria and Zangooee [22] numeri-

cally studied the capability of improving the cooling performance of vortex tube by using a divergent hot tube. Pourmahmoud *et al.* [23, 24] investigated the effect of operating pressure and injection lateral outflow on the performance of vortex tube.

CFD models can play an important role to elevate our understanding about different phenomena by providing significant insight into the flows. However, it is essential to evaluate the model predictions with the experimental data before using the model predictions for optimization or other purposes. In the present study, a 2-D axisymetric model along with four low cost two-equation turbulence models, namely the Standard k-ε, RNG k-ε, Realizable k-ε, and Standard k-ω model have been used to simulate the energy separation phenomenon in the RHVT used by Skye *et al*. [9]. By drawing a comparison between the numerical results and the published experimental and numerical data, we can arrive at the best two equation turbulence model for our investigation. Other RANS turbulence models such as the RSM solve additional equations when compared with the abovementioned two-equation models, thus involving high computational cost. The distributions of temperature, pressure, and components of velocity have been obtained in order to understand the flow behavior inside the tube.

Past experimental studies show that the maximum refrigeration capacity and the adiabatic efficiency of a RHVT always fall within the range of 50-70% cold mass fraction, irrespective of the diameter of the cold outlet [25, 26]. Nimbalkar and Muller [26] tried to explain this issue by considering the movement of the stagnation point inside the tube. In this study numerical simulation was carried out to study the effect of cold outlet diameter on cooling performance and refrigeration capacity of a RHVT. Furthermore, the movement of stagnation point at different cold mass fractions was investigated to examine the hypothesis proposed by Nimbalkar and Muller. Also, the relationship between the location of stagnation point and the maximum temperature point inside the tube was investigated. Recently, Eiamsa-ard *et al*. [27] utilized a RHVT in conjunction with a cooling system in order to improve the cooling performance of this device. In the present work the effect of using the cooling system was investigated numerically and the reason of improvement in cooling performance was explained by calculating the rate of energy transfer between the cold and hot regions inside the tube.

CFD simulation

Numerical modeling of the vortex tube was carried out by assuming an axisymetric steady-state flow. The working fluid was air which was considered as an ideal gas. The governing equations consist of the conservation of mass, momentum, and energy are written as:

$$\frac{\partial}{\partial x_i}(\rho u_i) = 0 \tag{1}$$

$$\frac{\partial}{\partial x_j}(\rho u_i u_i) = -\frac{\partial P}{\partial x_i} + \frac{\partial}{\partial x_j}\left[2\mu S_{ij} - \frac{2}{3}\mu\delta_{ij}\frac{\partial \mu_i}{\partial x_i}\right] + \frac{\partial}{\partial x_j} - (\overline{\rho u_1' u_3'}) \tag{2}$$

where, δ_{ij} is unit tensor and mean strain rate S is defined as:

$$s_{ij} = \frac{2}{3}\left(\frac{\partial u_i}{\partial x_j} + \frac{\partial u_i}{\partial x_j}\right) \tag{3}$$

$$\frac{\partial}{\partial x_i}[u_i(\rho E + P)] = \frac{\partial}{\partial x_j}\left[k_{\text{eff}}\frac{\partial u_i}{\partial x_j} + u_i(\tau_{ij})_{\text{eff}}\right] \tag{4}$$

where, k_{eff} is the effective thermal conductivity and $(\tau_{ij})_{\text{eff}}$ – the stress tensor which is defined as:

$$(\tau_{ij})_{\text{eff}} = 2\mu_{\text{eff}}\delta_{ij} - \frac{2}{3}\mu_{\text{eff}}\left(\frac{\partial u_{\text{k}}}{\partial x_{\text{k}}}\right)\delta_{ij} \tag{5}$$

The state equation for an ideal gas is:

$$P = \rho \text{R} T \tag{6}$$

In order to close the system of equations we need to model the terms $-\overline{\rho u_{\text{I}}' u_{\text{J}}'}$ in eq. 2. These terms are called Reynols stresses. The Boussinesq hypothesis is the most popular method to model the Reynols stresses via introducing an eddy viscosity:

$$-\overline{\rho u_{\text{I}}' u_{\text{J}}'} = 2\mu_{\text{t}} S_{ij} - \frac{2}{3}\mu\delta_{ij}\left(\rho k + \mu_{\text{t}}\frac{\partial u_{\text{k}}}{\partial x_{\text{k}}}\right) \tag{7}$$

There are several turbulence models to calculate the turbulent viscosity, μ_{t}. Two equation turbulence models are the simplest complete models for investigating turbulent flow, since by solving two separate transport equations, the turbulence velocity and length scale can be independently determined. In the present study four two-equation turbulence models namely the Standard k-ε, RNG k-ε, Realizable k-ε, and Standard k-ω models were used to identify the best model among them.

In Standard k-ε model the turbulence kinetic energy and the dissipation rate are obtained from the following transport equations:

$$\frac{\partial}{\partial t}(\rho k) + \frac{\partial}{\partial x_i}(\rho k u_i) = \frac{\partial}{\partial x_j}\left[\left(\mu + \frac{\mu_{\text{t}}}{\sigma_{\text{k}}}\right)\frac{\partial k}{\partial x_j}\right] + G_{\text{k}} + G_{\text{b}} - \rho\varepsilon - Y_{\text{M}} \tag{8}$$

$$\frac{\partial}{\partial t}(\rho\varepsilon) + \frac{\partial}{\partial x_i}(\rho\varepsilon u_i) = \frac{\partial}{\partial x_j}\left[\left(\mu + \frac{\mu_{\text{t}}}{\sigma_{\varepsilon}}\right)\frac{\partial_{\varepsilon}}{\partial x_j}\right] + C_{1\varepsilon}\frac{\varepsilon}{k}(G_{\text{k}} + C_{3\varepsilon}G_{\text{b}}) - C_{2\varepsilon}\rho\frac{\varepsilon^2}{k} \tag{9}$$

where G_{k} and G_{b} represent the generation of turbulence kinetic energy due to the mean velocity gradients and buoyancy, respectively. Y_{m} represents the contribution of the fluctuating dilatation in compressible turbulence to the overall dissipation rate.

The turbulent viscosity is computed using the following equation in which C_{μ} is a constant:

$$\mu_{\text{t}} = \rho C_{\mu}\frac{k^2}{\varepsilon} \tag{10}$$

The default constants were used in the present study:

$$C_{1\varepsilon} = 1.44,\ C_{2\varepsilon} = 1.92,\ C_{\mu} = 0.09,\ \sigma_k = 1.0,\ \text{and}\ \sigma_{\varepsilon} = 1.3$$

The RNG k-ε model is derived from instantaneous Navier-Stokes equations using mathematical technique known as the renormalization group (RNG) method. By considering the additional term in the ε equation and by using the analytically derived differential formula for effective viscosity, the accuracy of solution for rapidly strained flows and swirling flows, respectively, are expected to improve. Moreover, the RNG model in Fluent provides the option for considering the effect of swirl by modifying the turbulent viscosity [28]. In RNG k-ε model the turbulence kinetic energy and the dissipation rate are obtained from the following transport equations:

$$\frac{\partial}{\partial \mathrm{t}}(\rho k)+\frac{\partial}{\partial x_i}(\rho k u_i)=\frac{\partial}{\partial x_j}\left(\alpha_{\mathrm{k}}\mu_{\mathrm{eff}}\frac{\partial k}{\partial x_j}\right)+G_{\mathrm{k}}+G_{\mathrm{b}}-\rho\varepsilon-Y_{\mathrm{M}} \tag{11}$$

$$\frac{\partial}{\partial t}(\rho\varepsilon)+\frac{\partial}{\partial x_j}(\rho\varepsilon u_i)=\frac{\partial}{\partial x_j}\left(\alpha_{\varepsilon}\mu_{\mathrm{eff}}\frac{\partial \varepsilon}{\partial x_j}\right)+C_{1\varepsilon}\frac{\varepsilon}{k}(G_{\mathrm{k}}+C_{3\varepsilon}G_{\mathrm{b}})-C_{2\varepsilon}^{*}\rho\frac{\varepsilon^2}{k} \tag{12}$$

The turbulent viscosity is computed as:

$$\mathrm{d}\left(\frac{\rho^2 k}{\sqrt{\varepsilon\mu}}\right)=1.72\frac{\hat{V}}{\sqrt{\hat{V}^3-1+C_{\mathrm{V}}}}\mathrm{d}\hat{V} \tag{13}$$

where $\hat{V}=\mu_{\mathrm{eff}}/\mu$ and $C_{\mathrm{V}}\sim 100$.

At high Reynols numbers the turbulent viscosity is calculated as:

$$\mu_{\mathrm{t}}=\rho C_{\mu}\frac{k^2}{\varepsilon} \tag{14}$$

where $C_{\mu}=0.0845$ is derived using RNG theory. Because of considering the additional term in ε equation the last term at right hand side of this equation is different from the Standard k-ε model. In this term, $C_{2\varepsilon}^{*}$ is calculated as:

$$C_{2\varepsilon}^{*}=C_{2\varepsilon}+\frac{C_{\mu}\eta^3\left(\frac{1-\eta}{\eta_0}\right)}{1+\beta\eta^3} \tag{15}$$

where $\eta\equiv Sk/\varepsilon$, $\eta_0=4.38$, and $\beta=0.012$.

For weakly or moderately strained flows, the RNG model tends to give results comparable with the Standard k-ε model. However, for large strain rates, the value of $C_{2\varepsilon}^{*}$ is less than $C_{2\varepsilon}$ in the Standard k-ε model. As a result, the turbulent viscosity predicted by this model is less than the predicted value by the Standard k-ε model. The aim of this change was to make a model which is more responsive to the effects of rapid strain and stream line curvature than the Standard k-ε model.

The use of the new formula for turbulent viscosity and the new transport equation for the dissipation rate in the Realizable k-ε model, improves the probability of enhancing the solution for flows involving rotation, separation, and re-circulation.

In Realizable k-ε model the turbulence kinetic energy and the dissipation rate are obtained from the following transport equations:

$$\frac{\partial}{\partial t}(\rho k)+\frac{\partial}{\partial x_i}(\rho k u_i)=\frac{\partial}{\partial x_i}\left[\left(\mu+\frac{\mu_{\mathrm{t}}}{\sigma_{\mathrm{k}}}\right)\frac{\partial k}{\partial x_i}\right]+G_{\mathrm{k}}+G_{\mathrm{b}}-\rho\varepsilon-Y_{\mathrm{M}} \tag{16}$$

$$\frac{\partial}{\partial t}(\rho\varepsilon)+\frac{\partial}{\partial x_i}(\rho\varepsilon u_i)=\frac{\partial}{\partial x_j}\left[\left(\mu+\frac{\mu_{\mathrm{t}}}{\sigma_{\varepsilon}}\right)\frac{\partial \varepsilon}{\partial x_j}\right]+\rho C_1 S\varepsilon-\rho C_2\frac{\varepsilon^2}{k+\sqrt{\nu\varepsilon}}+C_{1\varepsilon}\frac{\varepsilon}{k}C_{3\varepsilon}G_{\mathrm{b}} \tag{17}$$

where $C_1=\max[0.43,\ \eta/(\eta+5)]$, $\eta=S(k/\varepsilon)$, $S=(2S_{ij}S_{ij})^{1/2}$.

The turbulent viscosity in this model is computed with the same equation as the Standard and RNG k-ε models. However, C_{μ} is no longer constant. This coefficient is computed as:

$$C_{\mu}=\frac{1}{A_{\mathrm{o}}+A_{\mathrm{s}}\frac{kU^{*}}{\varepsilon}} \tag{18}$$

$$U^* = \sqrt{S_{ij}S_{ij} + \widetilde{\Omega}_{ij}\widetilde{\Omega}_{ij}} \tag{19}$$

where $\widetilde{\Omega}_{ij} = 2\varepsilon_{ij}\omega_k$, $\Omega_{ij} = \overline{\Omega}_{ij} - \varepsilon_{ij}\omega_k$, $A_0 = 4.04$, $A_s = \sqrt{6}\cos\Phi$

$$\Phi = \frac{1}{3}\cos^{-1}(\sqrt{6}W),\ W = \frac{S_{ij}S_{jk}S_{ki}}{\widetilde{S}^3},\ \widetilde{S} = \sqrt{S_{ij}S_{ij}},\ S_{ij} = \frac{1}{2}\left(\frac{\partial u_j}{\partial x_i} + \frac{\partial u_i}{\partial x_j}\right)$$

In the Standard k-ω model, turbulent viscosity (μ_t) is computed by combining k and ω. This model has been modified for low Reynolds number effects, compressibility, and shear-flow spreading [28]. The turbulence kinetic energy, k, and the specific dissipation rate, ω, are obtained from the following transport equations:

$$\frac{\partial}{\partial t}(\rho k) + \frac{\partial}{\partial x_i}(\rho k u_i) = \frac{\partial}{\partial x_j}\left[\left(\mu + \frac{\mu_t}{\sigma_k}\right)\frac{\partial k}{\partial x_j}\right] + G_k - Y_k \tag{20}$$

$$\frac{\partial}{\partial t}(\rho\omega) + \frac{\partial}{\partial x_i}(\rho\omega u_i) = \frac{\partial}{\partial x_j}\left[\left(\mu + \frac{\mu_t}{\sigma_\omega}\right)\frac{\partial \omega}{\partial x_j}\right] + G_\omega + Y_\omega \tag{21}$$

In these equations, G_k represents the generation of turbulence kinetic energy due to mean velocity gradients. G_ω represents the generation of ω. Y_k and Y_ω represents the dissipation of k and ω due to the turbulence. The turbulent viscosity, μ_t, is computed by combining k and ω as:

$$\mu_t = \alpha^* \frac{\rho k}{\omega} \tag{22}$$

The coefficient α^* is responsible of low-Reynolds corrections. This coefficient is given by:

$$\alpha^* = \alpha_\infty^* \left(\frac{\alpha_0^* + \frac{\mathrm{Re}_t}{R_k}}{1 + \frac{\mathrm{Re}_t}{R_k}}\right) \tag{23}$$

where $\mathrm{Re}_t = \rho k/\mu\omega$, $R_k = 6$, $\alpha_0^* = \beta_i/3$, $\beta_i = 0.072$

At high Reynolds number form of the k-ω model, $\alpha^* = \alpha_\infty^* = 1$.

The 2-D, axisymmetric swirl model shown in fig. 2 was studied using Fluent 6.3.26 [28]. Gambit 2.3.16 [29] was used to generate the grid, which comprised of 29000 quad cells, with refinement near the wall, inlet, and outlets. In order to check the grid independency, computation for grids with 52000 and 102000 cells, was carried out, but the difference among the results was insignificant. The detail of the used geometry is presented in tab. 1. Instead of radial hot outlet used by Skye *et al*, the axial hot outlet was considered in this study which is more compatible with the experiment. At the inlet, a circumferential slot was assumed in place of the actual six inlet nozzles. As mentioned, previous studies indicate that in numerical modeling of a vortex tube with more than four nozzles, an axisymmetric model can be used instead of the 3-D model [13]. Nevertheless, a 3-D modeling

Figure 2. 2-D axisymetric configuration of the RHVT used in present study

of vortex tube used by Skye *et al*, was also carried out. The 3-D grid consists of 2,337,200 hexahedral cells is shown in fig. 3. The 3-D geometry has the same dimensions as the 2-D mode. However, instead of the circumferential slot the actual six straight inlet nozzles with 0.97 mm height, 1.41 mm width and 3.07 mm length were considered. Using a 3-D model could be a significant help to specify the components of the velocity at the inlet as well as finding an equivalent height of the inlet of the axisymetric model.

Table 1. The description of the 2-D model used in this study

Length of vortex tube	106 mm
Radius of tube	5.7 mm
Radius of cold outlet	3.1 mm
Radius of hot outlet	5.5 mm
Tangential component of velocity at the inlet	0.974 $\vec{V}$
Radial component of velocity at the inlet	–0.225 $\vec{V}$
Inlet height	1 mm

Numerical computations with boundary conditions of mass flow inlet at the inlet and pressure outlet at the outlets of RHVT were performed. The mass flow and the stagnation temperature at the inlet were 0.00835 kg and 294.2 K, respectively [30].The pressure at the cold outlet was set to the experimental values reported by Skye [30]. Simulations were conducted for different cold mass fractions by changing the hot end pressure. Coupled procedure was used to simultaneously solve the momentum and energy equations. The numerical solution was determined by first adopting the first-order upwind scheme, and after appropriate convergence, the second-order upwind scheme was used to discretize the convective terms of the governing equations. In addition to these, other schemes such as QUICK and third-order MUSCL were used. However, the difference between the results obtained was insignificant. In order to ensure the stability and convergence of the iterative calculation, lower under-relaxation factors and Courant numbers ranging from 0.008 to 0.4 and 0.5 to 2, respectively, were chosen. The global energy and mass balance for all the conditions were verified. The computations were performed in parallel using eight cores of Xeon E5530 CPU equipped with 24 GB memory RAM. The computational time for the 3-D model was around 130 hours. However, for the 2-D model it took around 4 hours.

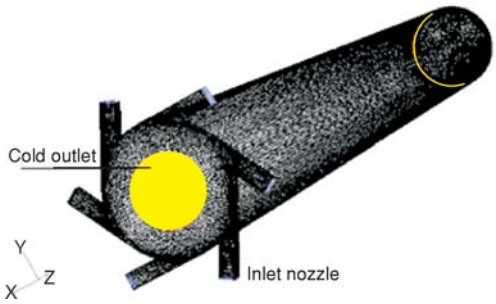

Figure 3. 3-D model of the RHVT used in this study

Result and discussion

Figure 4 illustrates a comparison between the present numerical results obtained by a 2-D axisymetric model and the previous experimental and numerical data. By drawing a compari-

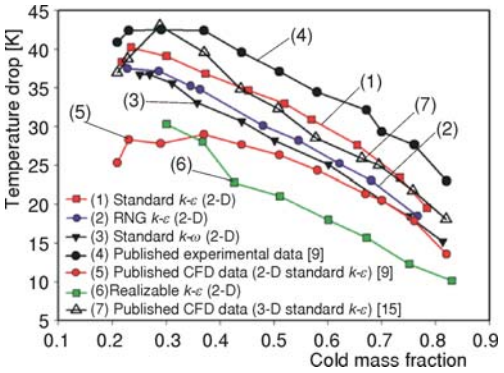

Figure 4. Comparison of the predicted temperature drop at the cold outlet by different turbulence models in this study and the published numerical and experimental data

son the Standard k-ε model was found to be better than the other models in predicting the total temperatures at the cold and hot outlets. Since the objective of this study is to investigate the cooling performance of the RHVT, the results for the hot outlet have not been reported for the sake of brevity. As mentioned, a full 3-D model was also developed in this study to identify the inlet boundary condition with more precision. The 3-D solution was performed for only few cold mass fractions and due to the similarity between the obtained results and the published data of Bramo and Pourmahmoud the published data was used for the comparison. From this figure, it is seen that there is a good agreement between the present 2-D results obtained by the Standard k-ε model and the published 3-D data presented by Bramo and Pourmahmoud [15]. Figure 5 shows the distribution of the total pressure at different axial locations in the radial direction. This figure indicates a significant radial pressure gradient with a higher pressure at the wall and a lower at the axis. This trend was observed in all the models. As seen there is a good agreement between the present results and the published 3-D data [15].

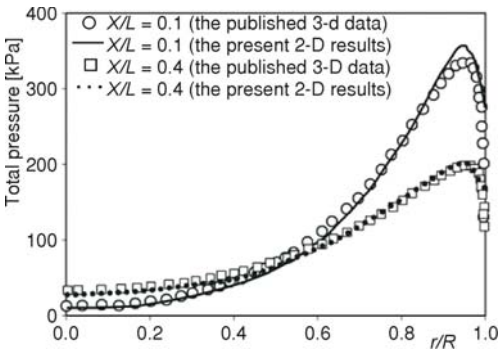

Figure 5. Distribution of total pressure as predicted by the present model (Standard k-ε) and published numerical results [15] for α = 0.3

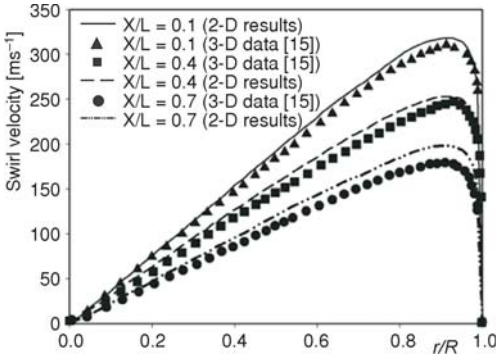

Figure 6. Distribution of swirl velocity in the radial direction as predicted by the present model and the published numerical results [15] for α = 0.3

By comparing the magnitude of the velocity components, it was observed that the magnitude of swirl velocity is the highest in all the models. According to fig. 6, the magnitude of swirl velocity decreases rapidly from the inlet to the hot outlet.

The distribution of the swirl velocity indicates that the swirl velocity increases in the radial direction, except at locations very close to the wall. A small discrepancy between the present 2-D results and the published 3-D data may be attributed to the small difference between the cold mass fractions because the cold mass fraction of the published 3-D data is not exactly equal to 0.3. Figure 7 illustrates the distribution of the angular velocity as predicted by the Standard k-ε model. According to this figure, the angular velocity decreases in the radial direction.

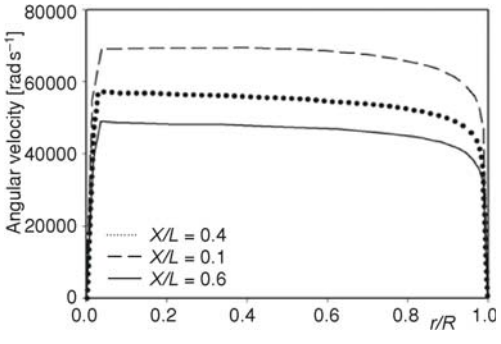

Figure 7. Prediction of angular velocity (ω) for the different sections by the Standard k-ε model (for α = 0.3)

This trend was observed in all the models, except in the RNG k-ε model, in which the magnitude of reduction in the radial direction was significantly higher than that in the other models. Figure 8 depicts the distribution of angular velocity as predicted by the RNG k-ε model. The value predicted by the RNG k-ε model for angular velocity near the axis is higher than that predicted by the other models. The distribution of the angular velocity indicates a transfer of shear work from the cold inner region to the hot peripheral region in the radial direction.

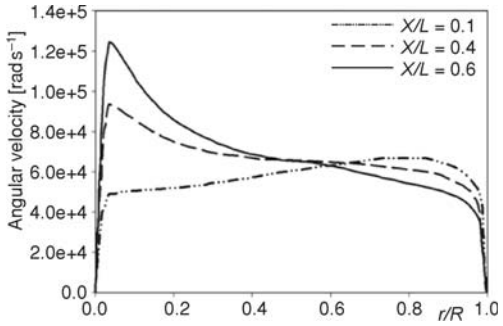

Figure 8. Prediction of angular velocity (ω) for the different sections by the RNG k-ε model (for α = 0.3)

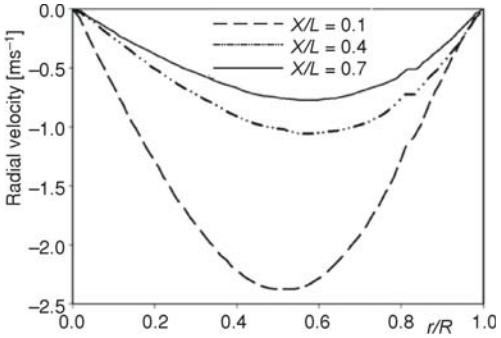

Figure 9. The profile of radial velocity as predicted by the Standard k-ε (for α = 0.3)

Figure 9 illustrates the prediction of the radial velocity by the Standard k-ε model in different sections of the tube. From this figure, it is obvious that the magnitude of radial velocity is very small when compared to the magnitude of the other components of velocity.

Figure 10 illustrates the radial distribution of axial velocity in different sections of the tube, as obtained by using the present 2-D model and published 3-D model. According to this figure, when the reverse flow goes to the cold outlet, the axial velocity and the diameter of the back flow increase. The profiles of the axial velocity in all turbulence models were very similar, except in RNG k-ε model, in which the magnitude of the axial velocity at the axis was significantly higher than the other models. This discrepancy was also observed in previous works [18, 21].

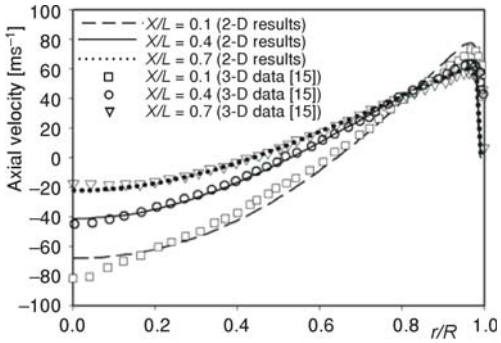

Figure 10. Radial distribution of axial velocity as predicted by the present results (Standard k-ε model) and the published numerical data [15] (for α = 0.3)

As mentioned, the distribution of the angular velocity indicates a transfer of viscous shear work from cold region to the hot peripheral region. In spite of the higher gradient of angular velocity predicted by the RNG k-ε model, the temperature drop predicted by this model is less than the predicted value by the Standard k-ε model. This issue is attributed to the level of turbulence predicted by these models. Figure 11 shows the radial distribution of turbulent viscosity as predicted by different turbulence models. As seen, the predicted value of turbulent viscosity by the Standard k-ε model is the highest. However, the RNG k-ε model predicted the minimum turbulent viscosity among all the models. From this figure, it is seen that the predicted

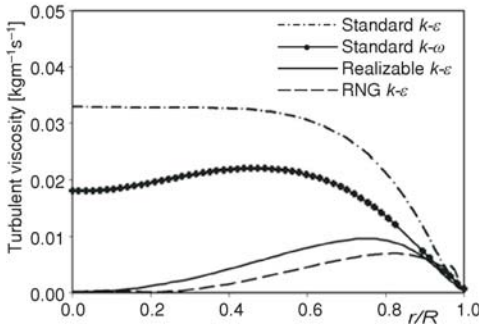

Figure 11. Prediction of the turbulent viscosity by the different turbulence models used in this study (for $\alpha = 0.3$)

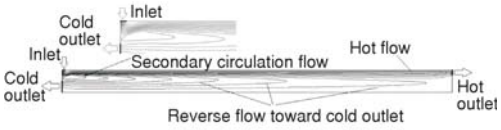

Figure 12. Streamlines within the RHVT as predicted by the Standard k-e model

Figure 13. Dividing stream line (cold mass fraction = 0.3)

value of the turbulent viscosity at the central region of the vortex tube is almost zero, indicating a laminar-like flow which contradicts the previous observations [31]. According to these results, the reason of predicting a significantly higher axial velocity by the RNG *k-ε* model can be attributed to the low turbulent viscosity and inadequate mixing. The turbulent viscosity plays an important role in transferring the viscous shear work from cold region to the hot region. Owing to the low magnitude of the turbulent viscosity predicted by the RNG *k-ε* model the viscous shear work transfer by this model is less than the predicted value by the Standard *k-ε* model, even though the gradient of the predicted angular velocity in this model is comparatively high.

The RNG formulated *k-ε* model is derived using RNG methodology of Yakhot and Orzag [32] and Yakhot and Smith [33] for the governing equations of turbulence. As mentioned, by considering the additional term in ε, it is expected to get a more realistic value for turbulent diffusivity. According to Pope [34] the additional term in the epsilon equation is an ad hoc model, which is not derived from RNG theory.The additional term changes dramatically with the strain rate of the turbulence and the turbulent diffusivity decreases significantly to obtain a more realistic behavior of flow-field. When such models are applied to a range of flows, the overall performance may be inferior to the standard model [34]. Previous applications of the original RNG *k-ε* model showed an unrealistic prediction of the mixing and turbulent viscosity which indicates a need to modify the model's coefficients for a particular physics of flow [35, 36].

Figure 12 illustrates the stream-lines within the RHVT as predicted by the Standard *k-ε* model. When the diameter of the cold outlet of the RHVT was set to the value used by Skye *et al*. [9], Secondary circulation flow was observed for all the cold mass fractions. According to the present results when the cold mass fraction and the diameter of the cold outlet are increased, the secondary circulation flow reduces. By using a specific stream-line, as shown in fig. 13, the flow field within the tube can be divided into hot and cold regions, so that the flow particles beyond this stream-line will exit from the hot outlet.

Figure 14 shows the radial distribution of static temperature at five axial locations of the tube as obtained by using the Standard k-e model. This figure shows a static temperature gradient near the inlet. This trend was observed in all the models.

The presence of a static temperature gradient can lead to heat transfer. From these figures, it can be seen that when we move away from the axis in the positive radial direction, the static temperature decreases. However, there exists a critical radius beyond which the static temperature dramatically increases. This sudden increase is due to the no slip boundary condition at

the wall of the tube. By considering the dividing stream-line shown in fig. 13, it can be concluded that when the radius of the dividing stream-line is less than the critical radius, the heat transfer on this stream-line is in the positive radial direction (toward the hot region). Therefore, this heat transfer can improve the energy separation effect. On the other hand, when the location of the dividing stream-line is beyond the critical radius, the direction of heat flux is reversed and this results in a heat loss in the hot region, which, in turn, leads to a reduction in the performance of the RHVT.

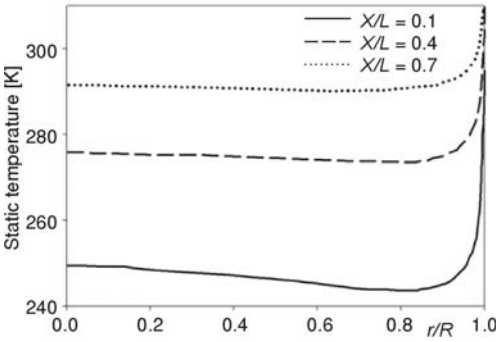

Figure 14. Radial distribution of static temperature as predicted by the Standard *k-ε* model (for α = 0.3)

Figure 15 shows the contours of the total temperature as predicted by the Standard *k-ε* model for the cold mass fraction of 0.3. All the turbulence models under-predicted the temperature drop at the cold outlet. With the exception of the magnitude of total temperature, the contours of the total temperature are very similar in all the models. Figure 16 illustrate the radial profiles of the total temperature as predicted by the

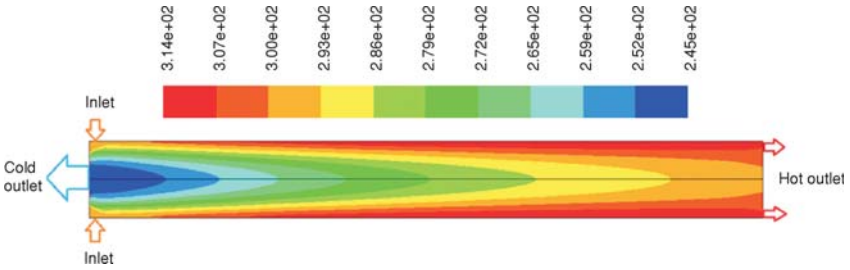

Figure 15. Contours of total temperature as predicted by the Standard *k-ε* model (for α = 0.3)

present 2-D model and the published 3-D data. From this figures, it is found that the maximum value of the total temperature is not located at the wall.

On the basis of the results obtained from the evaluation of the effectiveness of the abovementioned turbulence models, the Standard *k-ε* model was used to investigate the effect of the diameter of the cold outlet on the temperature drop at the cold outlet, which indicates the cooling performance of the RHVT. Therefore, numerical simulation was conducted for five different diameters of the cold outlet, in order to determine the optimum ratio between the cold outlet diameter and the internal diameter of the RHVT (*d/D*). All pa-

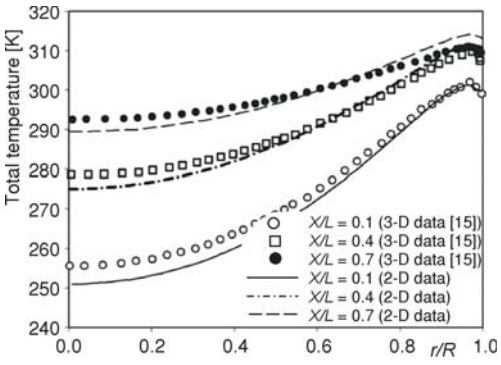

Figure 16. Radial distribution of total temperature as predicted by the Standard *k-ε* model (for α = 0.3)

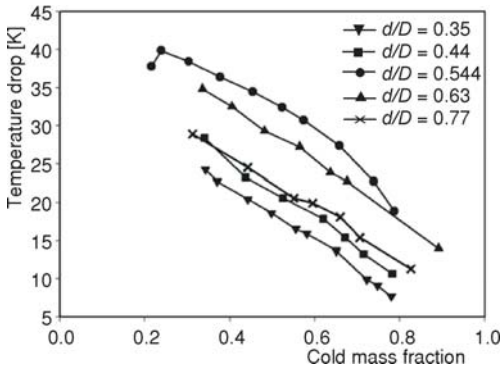

Figure 17. Effect of the diameter of cold outlet on the cooling performance of the RHVT

rameters, except *d/D*, were kept constant and the numerical simulations were performed for a constant mass flow rate at the inlet (0.00835 kg/s), which was measured by Skye *et al*. [9]. Figure 17 shows the results of the numerical simulation for five RHVT with different cold outlet diameters.

This figure indicates that there is an optimum value of *d/D*, such that, any increase or decrease in this ratio would result in a decrease in the temperature drop at the cold outlet. The numerical results indicate that the temperature drop is the highest in the RHVT having *d/D* = = 0.544. Previous experimental studies confirm this result [37, 38]. Moreover, according to our numerical simulation *d/D* has an important effect on the formation of secondary circulation flow: secondary circulation flow is larger at a low *d/D* ratio when compared to that a high *d/D* ratio.

In order to consider the effect of mass flow rate on the cooling performance of the RHVT, the refrigeration capacity at the cold outlet is defined as:

$$Q_c = \dot{m}_c c_p (T_i - T_c) \tag{24}$$

As mentioned, previous experimental studies show that the maximum refrigeration capacity and the adiabatic efficiency of a RHVT always falls within the range of 50-70% cold mass fraction, irrespective of the diameter of the cold outlet [25, 26]. As seen in fig. 18, the present numerical results confirm this observation. Nimbalkar and Muller [26] hypothesized that a change in the cold mass fraction causes a movement in the axial and radial stagnation points; an increase in the cold mass fraction moves the axial stagnation point toward the cold outlet, and at 60% cold mass fraction, the stagnation points move toward the optimum position at which the efficiency is the highest. However, in this study when we changed the cold mass fraction, there was no movement of the axial stagnation point. According to the present numerical results for the RHVT used by Skye *et al*. [9], the axial stagnation point is always positioned at the end of the tube, and this is due to the low *L/D* value in this RHVT. In order to study the effect of cold mass fraction on the movement of the stagnation point, numerical simulation was conducted on the RHVT having a higher *L/D* value. All parameters, except *L/D*, were kept constant, and numerical simulation was carried out for *L/D* = = 17.54. Figure 19 illustrates the movement of the axial stagnation point within the tube. From this figure, it is obvious that when we increase the cold mass fraction, the axial stagnation point will move to the end of the tube; this result contradicts the abovementioned hypothesis. Experimental studies confirm the present numerical

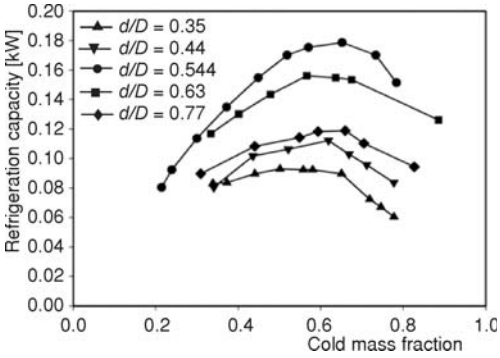

Figure 18. Refrigeration capacity (KW) *vs.* cold mass fraction for different values of *d/D*

results [39, 40]. The figure also shows the variation in the location of the maximum temperature point along the wall of the RHVT for different cold mass fractions. Previous experimental studies show that the position of the maximum temperature point also represents the axial stagnation point of the RHVT [41, 42]. Figure 19 supports this result. Figure 20 illustrates the refrigeration capacity at the cold outlet in the RHVT having $L/D = 17.54$. According to this figure, the refrigeration capacity had the maximum value at a cold mass fraction of approximately 65%.

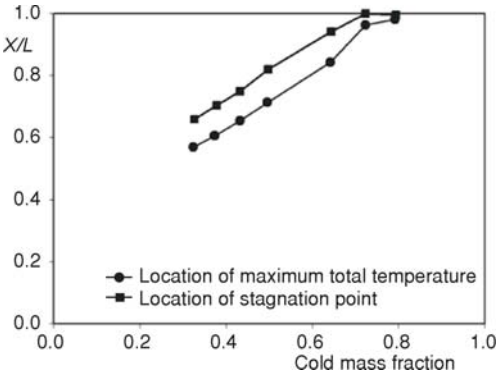

Figure 19. Effect of cold mass fraction on the location of stagnation and maximum temperature points

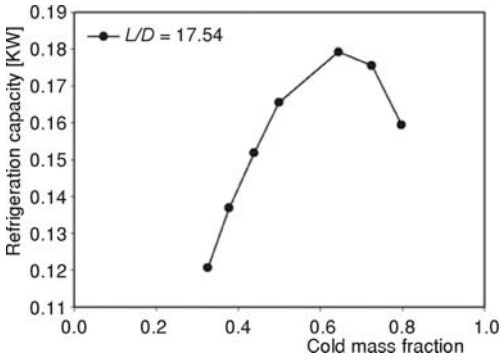

Figure 20. Cold power separation *vs.* cold mass fraction for RHVT with $L/D = 17.54$

As mentioned, Eiamsa-ard *et al.* [27] have tried to improve the cooling performance of a RHVT by utilizing this device in conjunction with a cooling system. As stated in this paper, the profile of static temperature in the radial direction indicates the existence of heat transfer between the cold inner region and the hot peripheral region. Therefore, it is expected that the use of the cooling system would change the heat transfer between the cold and hot regions.

In order to study the effect of cooling the hot tube, numerical simulation was conducted for three vortex tubes consisting of a cooling system, wherein the external wall of the RHVT was maintained at a temperature lower than that in the hot region. In this study, the temperature of the wall was constant at $T = 294.2$ K, 283 K, and 273 K. Figure 21 indicates that an increase in the cooling effect results in an increase in the temperature drop at the cold outlet; that is, when the temperature of the wall is 273 K, the temperature drop at the cold outlet is higher, when compared to the temperature drop at 283 K and 294.2 K. Moreover, it was observed that the reduction in the total temperature in hot region is significantly higher than the reduction in the total temperature in the cold region. In order to investigate the effect of the presence of the cooling system on the heat and work transfers between the cold and hot regions, the energy transfer between these regions was calculated by using the dividing streamline.

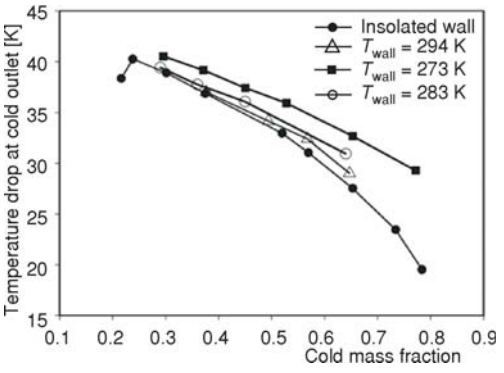

Figure 21. Effect of cooling of the tube on the cooling performance of the RHVT

The heat transfer per unit length is given by:

$$Q = -K_{\text{eff}} 2\pi r \frac{\partial T}{\partial n} \tag{25}$$

where K_{eff} is the effective thermal conductivity, T – the static temperature, and n – the normal direction on the dividing streamline.

The work transfer due to the viscous shear in tangential direction is computed according to:

$$W_{\text{t}} = -2\pi\mu_{\text{eff}} r u_\theta \frac{\text{d}\omega}{\text{d}n} \tag{26}$$

where μ_{eff} is the effective viscosity, u_θ – the swirl velocity, and ω – the angular velocity.

Work transfer due to the shear stress in axial direction is calculated by:

$$W_{\text{a}} = -2\pi\mu_{\text{eff}} r u_{\text{x}} \frac{\text{d}u_{\text{x}}}{\text{d}n} \tag{27}$$

where u_{x} is the axial velocity.

Figures 22 illustrates the energy transfer between the cold and hot regions for two RHVT with and without cooling systems at cold mass fraction of 66%. In these figures, the positive zones indicate that the energy transfer is from the cold region to the hot region and the negative zones indicate that the energy transfer is from the hot region to the cold region. According to these figures in this vortex tube at cold mass fraction of 0.66, heat transfer and axial work transfer are from hot region to the cold region and degrade the cooling performance of the vortex tube. However, the tangential work transfer is from cold region to the hot region and improves the cooling performance of RHVT. By comparing these figures, it is seen that due to the using cooling system the axial and tangential work transfers do not change. However, when cooling system is utilized the heat transfer between cold and hot regions changes. According to this figure, by utilizing the cooling system the negative zone area (heat transfer from hot region to the cold region) slightly decreases, thereby improving the cooling performance of the RHVT.

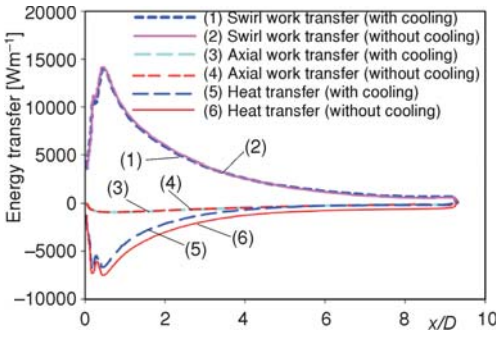

Figure 22. Axial work transfer between cold and hot regions at cold mass fraction of 66% (insolated wall)

Conclusions

In this study, a comparison among four two-equation turbulence models, namely, the Standard k-ε, RNG k-ε, Realizable k-ε, and Standard k-ω models, was drawn in order to identify the appropriate model for modeling the energy separation phenomenon in a RHVT. The results of the comparison between the experimental and numerical results show that the Standard k-ε model is better than other models in predicting the outlet temperatures. Furthermore, it was observed that a 2-D axisymetric model, accompanied with precise boundary conditions, could give comparatively good results with much less computational cost compared to the 3-D model.

The numerical results indicate that the magnitude of the radial velocity is insignificant when compared to those of the axial and swirl velocities. The distribution of angular velocity in

radial direction indicates the transfer of shear work from inner region to the peripheral region. The distribution of the static temperature confirms the existence of heat transfer between the cold inner region and the hot peripheral region. However, the direction of heat transfer depends on the location of the dividing stream-line.

The effect of *d/D* ratio on the cooling performance of the RHVT has been investigated by using the Standard *k-ε* model, and it was observed that by using a RHVT with $d/D = 0.544$, we can achieve the highest temperature drop and refrigeration capacity at the cold outlet. Furthermore, the present results indicate that maximum refrigeration capacity at the cold outlet always falls within the range of 50-70% cold mass fraction, irrespective of the *d/D* ratio.

The numerical results corresponding to the location of the stagnation point indicates that an increase in the cold mass fraction results in the movement of the stagnation point toward the hot outlet. The present numerical results contradict the hypothesis proposed by Nimbalkar and Muller. Moreover, it was observed that the position of the stagnation point represents the location of the maximum total temperature within the RHVT.

The effect of cooling the tube has also been studied, and the numerical results show that the cooling of the tube promotes the temperature drop at the cold outlet of the RHVT. The present numerical results indicate that by using a cooling system the rate of work transfer between cold and hot regions does not change. However, the heat transfer slightly changes. For the vortex tube used in this study using the cooling system resulted in decreasing the adverse heat transfer from hot region to the cold region, thereby improving the cooling performance of the RHVT.

Nomenclature

- c_p – specific heat capacity at constant pressure, [kJkg^{-1}K^{-1}]
- D – internal diameter of the RHVT, [mm]
- d – cold outlet diameter, [mm]
- k – turbulence kinetic energy, [m^{2}s^{-2}]
- L – length of the RHVT, [cm]
- $\dot{m}_c$ – mass flow rate at the cold outlet, [kgs^{-1}]
- Q – heat transfer, [Wm^{-1}]
- Q_c – refrigeration capacity at the cold outlet, [kW]
- T_c – total temperature at the cold outlet, [K]
- T_i – inlet temperature, [K]
- W – work transfer
- X – axial distance from cold outlet, [cm]

Greek symbols

- ε – turbulence dissipation rate, [m^{2}s^{-3}]
- μ_t – turbulent viscosity, [kgm^{-1}s^{-1}]
- ρ – density, [kgs^{-1}]

References

[1] Eiamsa-ard, S., Promvonge, P., Review of Ranque-Hilsch Effect in Vortex Tube, *Renewable and Sustainable Energy, 12* (2008), 7, pp. 1822-1842
[2] Ranque, G. J., Experiments on Expansion a Vortex with Simultaneous Exhaust of Hot Air and Cold Air (in French), *J. Phys. Radium, 4* (1933), 7, pp. 112-114
[3] Hilsch, R., The Use of Expansion of Gases in Centrifugal Field as a Cooling Process, *Review of Scientific Instruments, 18* (1947), 2, pp. 108-113
[4] ***, Method of Natural Gas Liquefaction (in Russian), Russia Patent RU 2202078, April 2003, http://www.sibpatent.ru/patent.asp?nPubl=2202078
[5] Bruno,T., Laboratory Applications of the Vortex Tube, *Canadian Journal of Chemical* Engineering, *Journal of Chemical Education, 64* (1987), 11, pp. 987-988
[6] Martin, R.W., Zilm, K.W.,Variable Temperature System Using Vortex Tube Cooling and Fiber Optic Temperature Measurement for Low Temperature Magic Angle Spinning NMR, *Journal of Magnetic Resonance, 168* (2004), 2, pp. 202-209

[7] Frohlingsdorf, W., Unger, H., Numerical Investigations of the Compressible Flow and Energy Separation in the Ranque-Hilsch Vortex Tube, *International Journal of Heat and Mass Transfer, 42* (1999), 3, pp. 415-422
[8] Aljuwayhel, N. F., *et al*., Parametric and Internal Study of the Vortex Tube Using a CFD Model, *International Journal of Refrigeration, 28* (2005), 3, pp. 442- 450
[9] Skye, H. M., *et al*., Comparison of CFD Analysis to Empirical Data in a Commercial Vortex Tube, *International Journal of Refrigeration, 29* (2006), 1, pp. 71-80
[10] Behera, U., *et al*., Numerical Investigation on Flow Behavior and Energy Separation in Ranque-Hilsch Vortex Tube, *International Journal of Heat and Mass Transfer, 51* (2008), 25-26, pp. 6077-6089
[11] Eiamsa-ard, S., Promvonge, P., Numerical Investigation of the Thermal Separation in a Ranque-Hilsch Vortex Tube, *International Journal of Heat and Mass Transfer, 50* (2007), 5-6, pp. 821-832
[12] Farouk,T., Farouk, B., Large Eddy Simulation of the Flow Field and Temperature Separation in Ranque-Hilsch Vortex Tube, *International Journal of Heat and Mass Transfer, 50* (2007), 23-24, pp. 4724-4735
[13] Shamsoddini, R., Hossein Nezhad, A., Numerical Analysis of the Effects of Nuzzle Number on the Flow and Power of Cooling of a Vortex Tube, *International Journal of Refrigeration, 33* (2010), 4, pp.774-782
[14] Hossein Nezhad, A., Shamsoddini, R., Numerical Three Dimensional Analysis of the Mechanism of Flow and Heat Transfer in a Vortex Tube, *Thermal Science, 13* (2009), 4, pp. 183-196
[15] Bramo, A. R., Pourmahmoud, N., Computational Fluid Dynamic Simulation of Length to Diameter Ratio Effects on the Energy Separation in a Vortex Tube, *Thermal Science, 15* (2011), 3, pp. 833-848
[16] Bramo, A. R., Pourmahmoud, N., A Numerical Study on the Effect of Length to Diameter Ratio and Stagnation Point on the Performance of Counter-Flow Ranque-Hilsch Vortex Tubes, *Australian Journal of Basic and Applied Sciences, 4* (2010), 10, pp. 4943-4957
[17] Pourmahmoud, N, Bramo, A. R., The Effect of L/D Ratio on the Temperature Separation in the Counter-Flow Vortex Tube, *International Journal of Research and Reviews in Applied Sciences, 6* (2011), 1, pp. 60-68
[18] Secchiaroli, A., *et al*., Numerical Simulation of Turbulent Flow in a Ranque-Hilsch Vortex Tube, *International Journal of Heat and Mass Transfer, 52* (2009), 23-24, pp. 5496-5511
[19] Pourmahmoud, N., *et al*., Numerical Analysis of the Effect of Helical Nozzles Gap on the Cooling Capacity of Ranque-Hilsch Vortex Tube, *International Journal of Refrigeration, 35* (2012), 5, pp. 1473-1483
[20] Pourmahmoud, N., *et al.*, Computational Fluid Dynamic Analysis of Helical Nozzles Effect on the Energy Separation in a Vortex Tube, *Thermal Science, 16* (2012), 1, pp. 151-166
[21] Dutta, T., *et al*., Comparison of Different Turbulence Models in Predicting the Temperature Separation in a Ranque-Hilsch Vortex Tube, *International Journal of Refrigeration, 33* (2010), 4, pp. 783-792
[22] Pouraria, H., Zangooee, M. R., Numerical Investigation of Vortex Tube Refrigerator with a Divergent Hot Tube, *Energy Procedia. 14* (2012), pp. 1554-1559
[23] Pourmahmoud, N., *et al*., Numerical Investigation of Operating Pressure Effect on the Performance of a Vortex Tube, *Thermal Science*, *18* (2014), 2, pp. 507-520
[24] Pourmahmoud, N., *et al*., Computational Fluid Dynamics Analysis of the Influence of Injection Nozzle Lateral out Flow on the Performance of Ranque-Hilsch Vortex Tube, *Thermal Science* 2013 Online First issue 00, pages: 2-2, DOI:10.2298/TSCI120704002P
[25] Poshernev, N. V., Khodorkov, I. L., Experience from the Operation of a Conical Vortex Tube with Natural gas, *Chemical and Petroleum Engineering, 39* (2003), 9-10, pp. 602-607
[26] Nimbalkar, S. U., Muller, M. R., An Experimental Investigation of the Optimum Geometry for the Cold end Orifice of a Vortex Tube, *Applied Thermal Engineering, 29* (2009), 2-3, pp. 509-514
[27] Eiamsa-ard, S., *et al*., Experimental Investigation on Energy Separation in a Counter-Flow Ranque-Hilsch Vortex Tube: Effect of Cooling a Hot Tube, *International Communications in Heat and Mass Transfer, 37* (2010), 2, pp. 156-162
[28] ***, Fluent User's Guide, Release 6.3.26, AnsysInc, USA, 2006
[29] ***, Gambit User's Guide, Release 2. 3. 16, AnsysInc, USA, 2006
[30] Skye, H. M., Comparison of CFD Analysis to Empirical Data in a Commercial Vortex Tube, B. Sc. thesis, University of Wisconsin, Madison, Wis., USA, 2006
[31] Xue, Y., *et al*., Experimental Study of the Thermal Separation in a Vortex Tube, http://dx.doi.org/10.1016/j.expthermflusci.2012.12.009

[32] Yakhot, V., Orszag, S. A., Renormalization Group Analysis of Turbulence. I. Basic Theory, *Journal of Scientific Computing, 1* (1986), 1, pp. 3-51
[33] Yakhot, V., Smith, L. M., The Renormalization Group, the Epsilon-Expansion and Derivation of Turbulence Models, *Journal of Scientific Computing,7* (1992), 1, pp. 35-61
[34] Pope, S. B., *Turbulent Flows*, Cambridge University Press, UK, 2000
[35] Han, Z., Reitz, R. D., Turbulence Modeling of Internal Combustion Engines Using RNG k-ε Models, *Combustion Science and Technology, 106* (1995), 4-6, pp. 267-295
[36] Amini, B., Khaleghi, H., A Comparative Study of Variant Turbulence Modeling in the Physical Behaviors of Diesel Spray Combustion, *Thermal Science, 15* (2011), 4, pp. 1081-1093
[37] Saidi, M. H.,Valipour, M. S., Experimental Modeling of Vortex Tube Refrigerator, *Applied Thermal Engineering, 23* (2003), 15, pp. 1971-1980
[38] Promvonge, P., Eiamsa-ard, A. S., Investigation on the Vortex Thermal Separation in a Vortex Tube Refrigerator, *Science Asia, 31* (2005), 3, pp. 215-223
[39] Ahlborn, B., Groves, S., Secondary Flow in a Vortex Tube, *Fluid Dynamics Research, 21* (1997), 2, pp. 73-86
[40] Gao, C. M., *et al*., Experimental Study on a Simple Ranque- Hilsch Vortex Tube, *Cryogenics, 45* (2005), 3, pp. 173-183
[41] Fulton, C. D., Ranque's Tube, *Journal of Refrigeration Engineering, 58* (1950), 5, pp. 473-479
[42] Aydin, O., Baki, M., An Experimental Study on Design Parameters of a Counterflow Vortex Tube, *Energy 31* (2006), 14, pp. 2763-2772

Paper submitted: June 10, 2012
Paper revised: April 7, 2013
Paper accepted: May 4, 2013